3D Modeling of Combustion in Lean Burn Four-Valve Engines : Influence of Intake Configuration

A.Torres and S.Henriot

Institut, Français du Pétrole
1&4, av. de Bois-Préau BP311, 92506 Rueil-Malmaison Cedx
France

ABSTRACT

The aim of this study is to predict the combustion phase in multi-valve engines. We compute, as a first application, the intake, compression and combustion strokes for two different intake configurations of a multi-valve engine at low fuel-air equivalent ratio. One head has a single operating intake valve while the other has two operating intake valves. We use a modified version of the KIVA-II code. The major enhancements are the implementation of a multi-block algorithm, an adaptive grid method, a remapping solver and the LI-CFM combustion model. We find some differences both on flow structure (tumbling motions and turbulence levels) and on flame propagation between the two configurations. As shown experimentally, a faster combustion velocity in the case of a single operating inlet valve is obtained.

INTRODUCTION

In the last few years, the amount of work on three dimensional simulations of spark ignition engines has been increasing. Many of these studies (1, 2) focused on the intake and compression stroke of four-valve engines. Others were related to the combustion phase, with different flamelet combustion models in flat-head chambers (3, 4, 5) or in pent-roof chambers with a EBU type model (6). But very few (7) have combined computation of intake/compression and combustion strokes in real-world geometries. The primary goal of this study is to perform such a computation. The second one is to be able to simulate the combustion in a lean-burn configuration. Several studies (8, 9) show the advantage of operating engines with a lean mixture, especially to reduce pollutant emissions (NO_x and CO) and specific fuel consumption. While the number of experimental studies is still growing, no numerical studies have yet been reported on this subject. Finally, the third goal is to show that, with only a numerical tool, we are able to predict well the differences in combustion propagation between two engines geometries (single and dual operating intake valve).

CONFIGURATIONS

The engine specifications adopted for this study are summarized in Table 1. Our two configurations differ only by the number of ports and valves: one for the "case I" and two for the "case II". For this purpose, two 3D meshes of a pent-roof combustion chamber are generated. The finite volume grids have 88,000 vertices in the cylinder and 4,000 in each pipe.

Bore x Stroke	8.6 x 8.6 cm
Compression ratio	10
RPM	2000
Fuel/air equivalence ratio	0.7, propane
BMEP	2 bar
Spark timing	40 deg. BTDC
Inlet Valve Opening (IVO)	20 deg. BTDC
Inlet Valve Closing (IVC)	50 deg. ABDC
Maximum valve lift	9.2 mm

Table 1 Engine specifications

Although computational meshes follow closely the shape of the engine configurations, minor simplifications have been made in the geometries and engine parameters. These include: only a part of valve stems are modeled; the spark plug hole is neglected; the first and the last 0.5 mm of the valve lift are not taken into account to avoid very thin cells or a single inflow cell; and the exhaust valves are assumed to be closed at the beginning of calculations.

At the same time, an experimental study was carried out. Cylinder and inlet pipe pressures were measured and will be used for comparisons.

COMPUTATIONAL APPROACH

The Original 3D Code

KIVA-II solves finite volume approximations of the average Navier-Stokes equations, coupled to a k-ε turbulence model. It can calculate transient, three dimensional, compressible, chemically reactive turbulent flows with sprays

and moving boundaries. The equations, the numerical scheme and the computer program are described in detail in (10).

Numerical Enhancements

The Multi-block algorithm. A multi-block structured code was developed on the KIVA-II code. By this technique, calculations in complex geometries are possible with a reasonable number of inactive cells, and hence reasonable computational time and storage requirements. The manner in which the different regions are linked by a fully conservative procedure is presented in (11). Compared to the original structured version of KIVA-II, and as in KIVA 3 (12), the reduction of inactive cells allows us to take into account manifolds for multi-valve engines or ports for two stroke engines (13) with more refined meshes. In the present study, the structured mesh would have had 135,000 vertices, instead of 92,000 for our multi-block configuration.

The auto-adaptive mesh method. An original auto-adaptive mesh method (14), based on an analogy with mechanical problems, is used. This iterative algorithm permits the motion of cells involved by moving boundaries (i.e. valves and piston displacement). It also ensures a uniform aspect ratio in all directions for each cell and a small difference in cell size for neighbouring cells.

The Remapping Code

One major problem with engine computation is that different phases of the calculations do not have the same mesh requirements: the intake phase needs a refined mesh near valves and pipes; the combustion stroke requires a uniform mesh and more refined, single row, uniform cells near walls. To meet these needs, we use an original remapping code which transfers quantities from one mesh to an other. This code is not as general as the code in (15), in the sense that the number of vertices in each direction of the "old" and the "new" mesh remains constant. This conservative code uses the Q.S.O.U. scheme, which approaches second-order accuracy. As an exemple, Fig. 1 illustrates the remapping of a vortex flow with a strong gradient in species concentrations from a mesh A to a mesh B. All validations show that with grid densities and gradients typical of engine configurations, the discrepancy between the original and remapped fields is lower than 5 %.

Initial and Boundary Conditions

Calculations begin at intake TDC. The pressure in the inlet mainfolds and in the cylinder are set to experimental values (they also might be set to 1D code values). Temperature and residual gas mass fraction are estimated to be 800 K and 0.55. We assume that there is no unburnt fuel inside the cylinder. Turbulent kinetic energy, k, is set equal to 10 % of the kinetic energy based on mean piston speed. The dissipation rate ε is set equal to $k^{3/2}/h$, where h is the half distance between the top of the cylinder head and the piston at TDC.

The slip condition at the wall of KIVA-II is extended to the complex shape of engines; and the turbulent law of the wall is modified to take into account the slipping velocity at the wall. We have also implemented the heat transfer law of Diwakar. The wall temperature is uniform in space and time during all the calculation, and is equal to 450 K. At inflow boundaries, the velocity profile is assumed to be uniform accross the inlet section of the pipe, and the mass flow rate is calculated from the pressure difference between the port and the upstream experimental values. We set the temperature to 300 K and the species concentration according to the air/fuel ratio. Turbulent variables are estimated from those of a steady state flow in a duct of the same diameter.

The Combustion Model

The combustion stroke is modeled with the LI-CFM model that was used in (4) and it is briefly described here. This model splits the combustion phases into three coupled parts:

The laminar ignition phase. During this phase, which is calculated outside KIVA by a 1D code (LI), ignition can be seen as a pseudo-laminar process. The LI model solves the full Navier-Stokes equations, at constant pressure, for a chemical

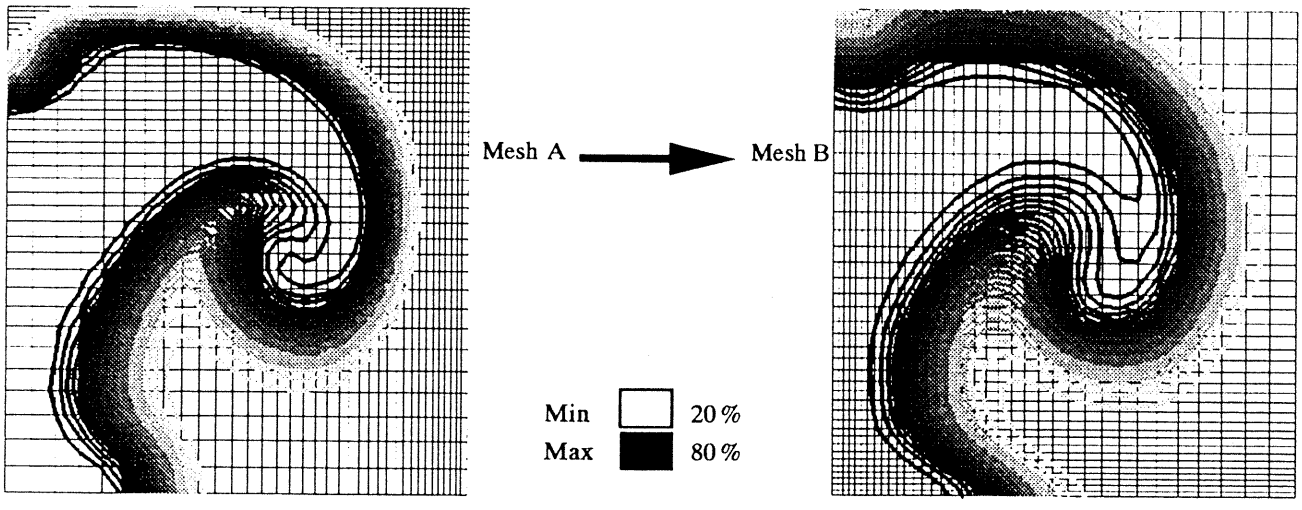

Fig.1 Species iso-concentration of a vortex flow in a box before and after the remapping phase

reaction controlled by an Arrhenius law. It requires as input parameters the flame characteristics, the ignition device characteristics and the thermodynamic conditions of the flow (provided by KIVA). It outputs the radius r_1 reached by the flame and the delay t_1 after which the laminar ignition ends.

This model does not take into account a flow velocity at spark plug location. In the present study, the deformation of the flame kernel is still neglected. We only correct the delay t_1 using the direct numerical simulation results of (16). this results give a spark duration time t_s as a fonction of: the flow velocity at spark location V_{spark}, the laminar flame speed s_l, the heating power, the laminar flame power and the delay t_1 with no flow speed.

The laminar-turbulent phase. In this second phase, computed with the 3D code, the flame kernel grows because of laminar effects but its surface is also stretched by turbulent eddies. Transition from this phase to the fully turbulent one is triggered at t_2 with a kernel radius r_2, when the turbulent flame stretch K_t is larger than the laminar flame stretch K_l. K_t is given by the ITNFS model (17) and is equal to:

$$K_t = (1/\Sigma)\, d\Sigma/dt = \varepsilon/k\ f(u'/s_l, L/l_f)$$

where Σ is the flame surface density, u' is the RMS turbulent velocity, L the integral lenght scale and l_f the flame thickness. The fonction f is given in (17). For the laminar stretch, we have:

$$K_l = 2\, T_2/T_1\, s_l/r$$

where T_1 and T_2 designate the temperature of the fresh and burnt gases and r the flame kernel radius.

The fully turbulent phase. It is modeled using a version of the Coherent Flame Model (CFM, 18). In this model, the mean turbulent reaction rate for the reactants may be expressed as the product of Σ by the consumption rate of fuel per unit of flame area. A balance equation is then written for Σ:

$$\frac{\delta\Sigma}{\delta t} + \frac{\delta u_i \Sigma}{\delta x_i} = \frac{\delta}{\delta x_i}\left(\frac{\nu_t\, \delta\Sigma}{\sigma_\Sigma \delta x_i}\right) + \alpha K_t \Sigma - \beta \frac{\omega_l (1 + ak^{1/2}/s_l)}{\rho Y} \Sigma^2$$

where Y is the local mean mass fraction of fuel, ω_l the consumption rate of fuel per unit of flame area, ν_t the turbulent diffusivity and ρ the density. Once again, the ITNFS model is used to estimate the flame rate K_t. The parameters of the model are those of (4), except for a slight difference for α (2.3 instead

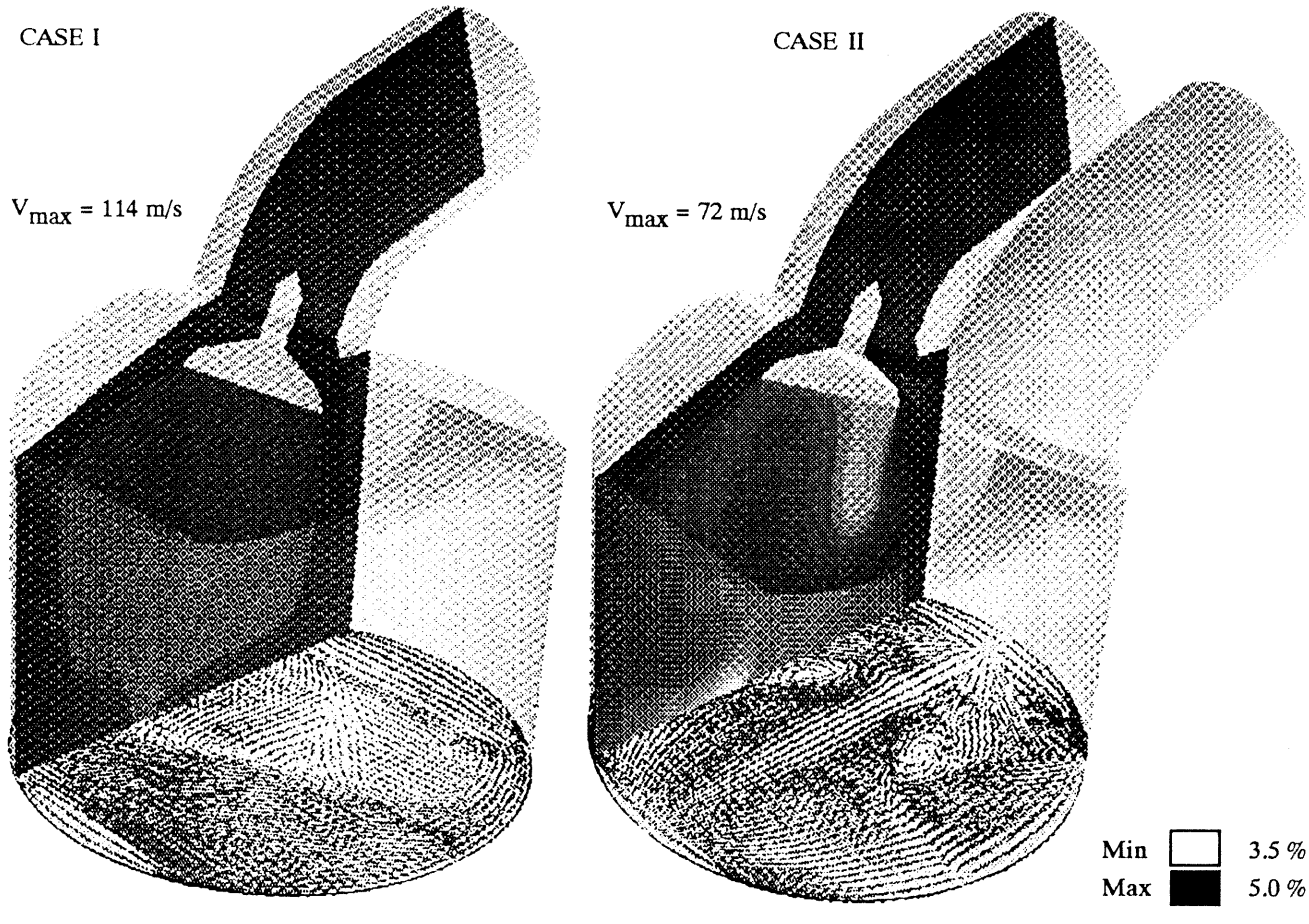

Fig. 2 Velocity and fuel mass fraction at 270° BTDC

of 2.1 previously) and a (0.15 instead of 0.1). This point will be dicussed below. β and σ_Σ are unchanged: $\beta = \sigma_\Sigma = 1$.

Σ is treated as a fictitious species in KIVA. Actually, combustion models can't describe accurately the combustion near wall since the ratio ε/k is not well predicted by the turbulence model. For this reason, as a first approximation, the production term $\alpha K_t \Sigma$ is set equal to zero in the boundary layer cell.

RESULTS AND DISCUSSION

The Intake Phase

Fig. 2 shows the fuel mass fraction field in a plane across the valve and the velocity field on the piston at mid intake. We notice some differences on flow structure between the two configurations : two counter-rotating small vortices begin to grow in case II, at each side of the plane of symmetry. In case I, the flow field is, at this time, complex and one inclined tumbling motion is generated, as previously observed in (1). Velocity intensities are higher in case I (maximum of 114 m/s vs 72 m/s for case II), as intake valve air passage area in case I is half the one of case II. In the scalar field, in both cases, the entering gases flow down along the cylinder head and walls, with two vortices under the valves. In this figure, fuel concentration seems to be more important in case I. This is due to the inflow configuration with one valve. After the intake valve is closed, the mixture in the both case has the same equivalence ratio and is quasi-homogeneous.

The compression and Ignition Phases

At the closing of valves (140 deg. BTDC), the two configurations are remapped to the same grid. We can see this grid in Fig. 3 later in the engine cycle. Note that pipes, valves and their trace in the computational domain are removed.

For both cases, the LI code gives $t_1 = 0.2$ ms for the delay and $r_1 = 1$ mm for the radius of the flame kernel at the end of the laminar phase. The extra-delay due to non-zero velocity at the spark plug location is zero for case II (i.e. $t_s = t_1$). This extra-delay is equal to $2.65t_1$ for case I (i.e. $t_s = 3.65t_1$). The amount of energy released by the spark being large and the flow velocity being small in case II (Fig.3, $V_{spark}/s_L = 6$ vs 12 in case I), we find that the flow velocity is not sufficient in case II to cause an extra-delay.

Time t_2, where the turbulent stretch balances the laminar one, is reached at 28.5 degrees BTDC for case II and 27.8 for case I. At those crank angles, we plot in Fig. 3 the turbulent kinetic energy in a plane located in the squish region. Two major observations may be noted. The first is that the turbulence level is almost two times higher in case I than in case II. The second is that the maximum of turbulent kinetic energy is not located in the same region for the two configurations. In case I, it is located in the center of the combustion chamber and for case II, it is distributed symmetrically under each intake valve. The maximum of turbulent energy always corresponds to the middle of an inclined tumble of the flow field. We will see that the way in which the turbulence intensity is distributed around the ignition location has a great influence on combustion propagation. At t_2, the initial flame surface density is deposited spherically (4) in the beginning of CFM's calculations. Because of a higher turbulent stretch in case I, the transition duration between t_s and t_2 is shorter. Consequently, the flame radius at t_2 is smaller with $r_2 = 2.4$ mm compared to $r_2 = 4.4$ mm in case II.

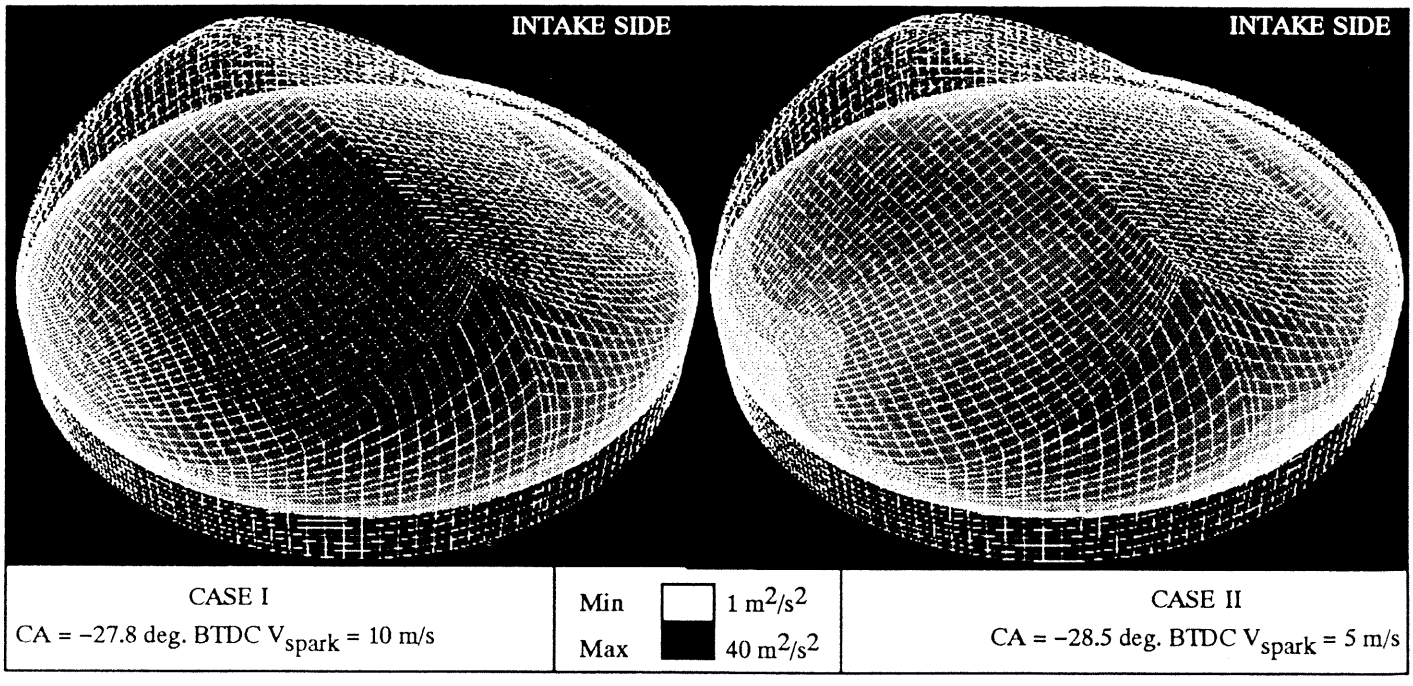

Fig. 3 Turbulent kinetic energy field before the fully turbulent combustion phase

The Combustion Phase

In Fig. 4, we show the flame surface density Σ at the same burnt mass fraction: 9%. Views A and C are planes which cross the chamber by the edge of the roof. Views B and D are planes perpendicular to A and C and which cross the middle of the spark plug. The intake side is located on the front of A and C, and in the right of B and D. The level of Σ is much higher in case I: because of the stronger turbulent flow, the flame surface is more stretched, which results in a higher combustion velocity. More specifically we can notice in case I that the flame seems to be pushed to the no-intake valve region of the chamber (left side on A view of Fig. 4): the flame front follows the shape of the flow field (i.e. one inclined tumble). It is the same for case II: the combustion propagation is symmetrical in the direction perpendicular to the edge of the cylinder head, but in the other direction (right side on D view of Fig. 4), the flame is pushed to the intake side of the chamber by the action of the two counter-rotating vortices.

The computed and measured pressure curves are showned in Fig. 5. They agree well: a higher maximum pressure and a better heat release rate are obtained in case I both for experiments and calculations. As it was found experimentaly (8), the most favorable configuration for lean burn operation is case I. It offers the advantages of inducing a more stable fluid motion and an optimal turbulence level. This is caused by the intake process with high velocities and by the breakdown of tumbling motion before TDC. In case II, the unstable gas motion and the low turbulence level result in a low burning rate and high cycle to

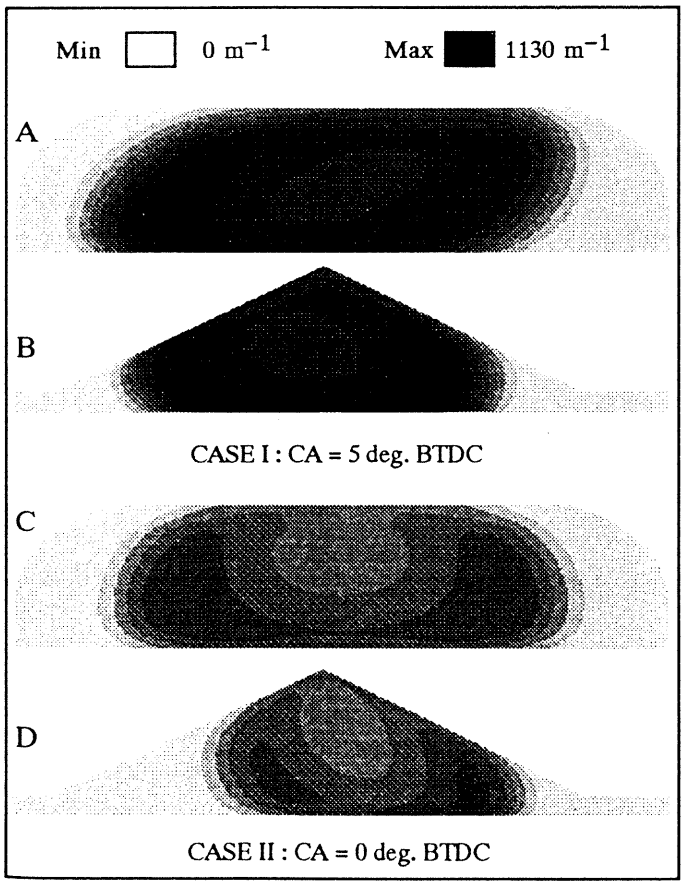

Fig. 4 Flame surface density fields at 9 % burnt mass fraction

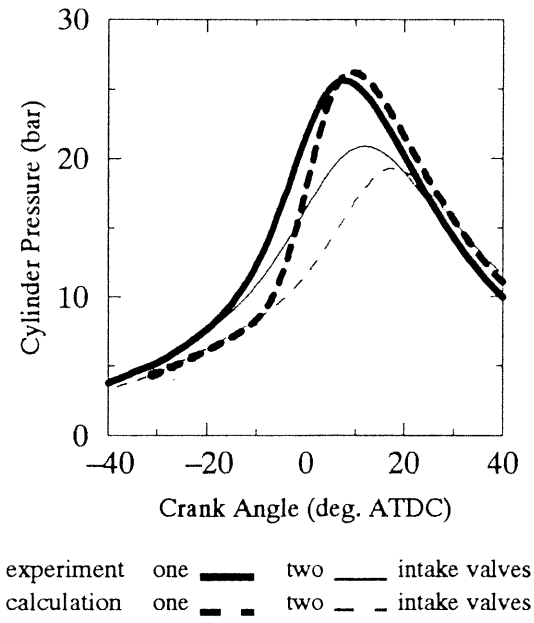

Fig. 5 Comparison of pressure laws

cycle variations under lean conditions.

While the agreement between model predictions and measurements is good (i.e. nearly the same level and location for the peak of pressure), some differences are noticed but may be explained. First, the entire inlet strokes are calculated: velocity and turbulence fields at ignition time are not fitted to experimental values as usualy (3, 4, 5, 6). We have to deal here with the resulting numerical and turbulence model approximations. Moreover, as can be seen in Fig. 5, the calculated pressure in the cylinder is under-estimated before combustion (~40 deg. BTDC). This is due to a poor estimate of the mass of residual burnt gases in the cylinder at the beginning of the calculation. For all these reasons, the values of some CFM's parameters had to be slightly modified to get a reasonable combustion level in case II.

Note that, in case II, the operating conditions (with an fuel-air equivalence ratio of 0.7) are near the lean limit. The experimental mean cylinder pressure does not reveal the very high cycle to cycle instability, as can be seen in Fig. 6. The combustion model can't reproduce such unstabilities.

CPU TIME

Intake computations take 3.6 hours for case II and 4 hours for case I on a Fujitsu VP 2400. The difference is caused by the higher velocities and gradients met in case I (i.e. smaller time step and higher number of sub-cycles in Eulerian phase). The compression stroke requires 2 hours. The computation time from the spark to the end of calculations (40 deg. ATDC) is 2.5 hours.

CONCLUSION

The calculation of intake, compression and combustion phases has been performed for four-valve engine considering

two intake configurations (one and two operating intake valves). The fluid motion of the two-intake-valve configuration is characterized by two counter-rotating vortices with inclined axes, while the one-intake -valve configuration is dominated by an inclined tumble and a high turbulence level.

During the combustion phase, calculation shows that the one valve configuration is most favorable to lean-burn operation, a trend confirmed by experiments. This is not due to inhomogeneity of the fuel in the cylinder, but rather to the flow configuration characterized by a higher turbulence level and a more stable fluide motion.

The LI-CFM combustion model which has been found to predict effects of spark timing, equivalence ratio and pressure is shown here to deal correctly with complex actual engine flows.

Although our calculations have to be improved both on fluid dynamics and combustion modeling (turbulence, ignition and flame-wall interaction), CFD codes can be now used to evaluate engine combustion performances.

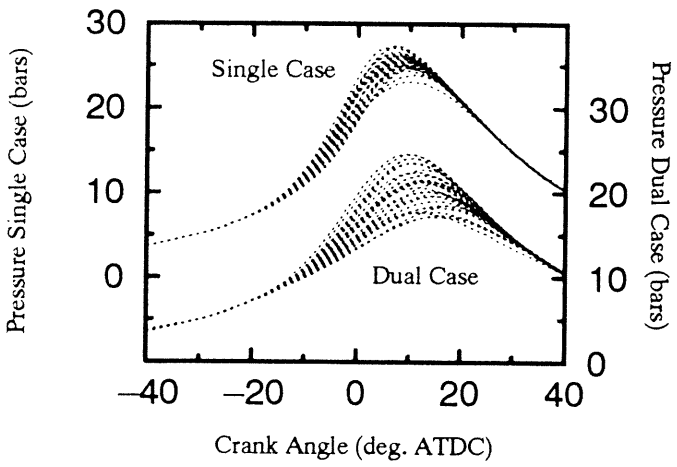

Fig. 6 Experimental pressure cyclic variations

ACKNOWLEDGEMENTS

The authors would like to express thank to M. Castagne (IFP) for providing the engine data and to Dr. P. Boudier for many helpfull discussions.

REFERENCES

1. Le Coz, J.-F., Henriot S., and Pinchon P., "An Experimental and Computational Analysis of the Flow Field in a Four-Valve Spark Ignition Engine. Focus on Cycle-Resolved Turbulence," SAE, Paper No. 900056, 1990.
2. Haworth, D. C., El Tahry, S. H., Huebler, M. S., and Chang, S., "Multidimensional Port-and-Cylinder Flow Calculations for Two and Four-Valve-Per-Cylinder Engines : Influence of Intake Configuration on Flow Structure," SAE, Paper No. 900257, 1990.
3. Cheng, W. K., and Diringer, J. A.,"Numerical Modelling of SI Engine Combustion with a Flame Sheet Model," SAE, Paper No. 910268, 1991.
4. Boudier, P., Henriot, S., Poinsot, T., and Baritaud, T., "A Model for Turbulent Flame Ignition and Propagation in Spark Ignition Engines," Twenty-Fourth Symposium (International) on Combustion, pp. 503-510, 1992.
5. Zhao, X., Matthews, R. D., and Ellzey, J. L., "Three-Dimensional Numerical Simulation of Flame Propagation in Spark Ignition Engines," SAE, Paper No. 932713, 1993.
6. Najt, P. M., and Kuo, T. W., "An Experimental and Computational Evaluation of Two Dual-Intake-Valve Combustion Chambers," SAE, Paper No. 902140, 1990.
7. Naitoh, K., Takagi, Y., and Kuwahara, K., "Cycle-Resolved Computation of Compressible Turbulence and Premixed Flame in an Engine," Computers and Fluids, Vol. 22, No. 4/5, pp. 623-648, 1993.
8. Le Coz, J.-F., Henriot, S., Herrier, D., Marie, J.-J., and Barret, P., "Development of a Lean Burn Multi-Valve S.I. Engine : a New Approach Based on Flow Field Optimization," SIA, Paper No. 91012, 1991.
9. Kiyota, Y., Akishino, K., and Ando, H., "Concept of Lean Combustion by Barrel-Stratification," SAE, Paper No. 920678, 1992.
10. Amsden, A. A., O'Rourke,P. J., and Butler,T. D., "KIVA 2, a Computer Program for Chemically Reactive Flows with Sprays," Report LA-11560-MS, Los Alamos National Laboratory, 1989.
11. Habchi, C., and Torres, A., "A 3D Multi-Block Structured Version of the KIVA 2 Code," First European CFD Conference proceedings, pp. 502-512, 1992.
12. Amsden, A. A., " KIVA-3: A KIVA Program with Block-Structured Mesh for Complex Geometries," Report LA-12503-MS, Los Alamos National Laboratory, 1993.
13. Habchi, C., and Baritaud, T., "Contribution of 3D CFD Studies to the Design Cycles of New 2 Stokes DI Engines," ISATA proceedings, Paper No 93SC018, pp. 103-114, 1993.
14. Fabre, A., Fattal, M., Kennel, C., Argueyrolles, B., Bailly, C., Buchou, C., Henriot, S., Stoessel, A., Torres, A., and Hallot, J., "Code de Calcul GSM : Compte Rendu des Travaux Effectues en 1992," Rapport 40517, Institut Francais du Petrole, 1993.
15. Dukowicz, J. K., and Padial, N. T., "REMAP3D : A Conservative Three-Dimensional Remapping Code," Report LA-12136-MS, Los Alamos National Laboratory, 1991.
16. Baum, M., and Poinsot, T., "Effects of Mean Flow on Premixed Flame Ignition," Submitted to the 25th. Symposium (International) on Combustion, 1994.
17. Meneveau, C., and Poinsot, T., "Stretching and Quenching of Flamelets in Premixed Turbulent Combustion," Combustion and Flame 86, pp. 311-332, 1991.
18. Candel, S., Veynante, D., Lacas, F., Maistret, E., Darabiha, N., and Poinsot, T., "Coherent Flame Model: Applications and Recent Extensions," Recent Advances in Combustion Modelling, B. Larrouturou Ed., World Scientific, Singapore, 1990.